A comparative study of capacitively coupled HBr/He, HBr/Ar plasmas for etching applications: Numerical investigation by fluid model

ARTICLE *in* PHYSICS OF PLASMAS · OCTOBER 2015

Impact Factor: 2.14 · DOI: 10.1063/1.4934922

2 AUTHORS:

Banat Gul

Pakistan Institute of Engineering and Applie…

3 PUBLICATIONS **1** CITATION

SEE PROFILE

Aman ur Rehman

Pakistan Institute of Engineering and Applie…

23 PUBLICATIONS **46** CITATIONS

SEE PROFILE

A comparative study of capacitively coupled HBr/He, HBr/Ar plasmas for etching applications: Numerical investigation by fluid model

Banat Gul and Aman-ur-Rehman

Citation: Physics of Plasmas **22**, 103520 (2015); doi: 10.1063/1.4934922
View online: http://dx.doi.org/10.1063/1.4934922
View Table of Contents: http://scitation.aip.org/content/aip/journal/pop/22/10?ver=pdfcov
Published by the AIP Publishing

A comparative study of capacitively coupled HBr/He, HBr/Ar plasmas for etching applications: Numerical investigation by fluid model

Banat Gul[1,2,a)] and Aman-ur-Rehman[1,b)]
[1]*Department of Physics and Applied Mathematics, Pakistan Institute of Engineering and Applied Sciences, Nilore, Islamabad 45650, Pakistan*
[2]*Research Group PLASMANT, Department of Chemistry, University of Antwerp, Universiteitsplein 1, B-2610 Antwerp, Belgium*

(Received 20 August 2015; accepted 16 October 2015; published online 29 October 2015)

Fluid model has been applied to perform a comparative study of hydrogen bromide (HBr)/He and HBr/Ar capacitively coupled plasma discharges that are being used for anisotropic etching process. This model has been used to identify the most dominant species in HBr based plasmas. Our simulation results show that the neutral species like H and Br, which are the key player in chemical etching, have bell shape distribution, while ions like HBr^+, Br^+, which play a dominant rule in the physical etching, have double humped distribution and show peaks near electrodes. It was found that the dilution of HBr by Ar and/or He results in an increase in electron density and electron temperature, which results in more ionization and dissociation and hence higher densities of neutral and charged species can be achieved. The ratio of positive ion flux to the neutral flux increases with an increase in additive gas fraction. Compare to HBr/He plasma, the HBr/Ar plasma shows a maximum change in the ion density and flux and hence the etching rate can be considered in the ion-assisted and in the ion-flux etch regime in HBr/Ar discharge. The densities of electron and other dominant species in HBr/Ar plasma are higher than those of HBr/He plasma. The densities and fluxes of the active neutrals and positive ions for etching and subsequently chemical etching versus physical sputtering in HBr/Ar and HBr/He plasmas discharge can be controlled by tuning gas mixture ratio and the desire etching can be achieved. © *2015 AIP Publishing LLC*.
[http://dx.doi.org/10.1063/1.4934922]

I. INTRODUCTION

Low temperature and low pressure plasma discharges have been widely used in the semiconductor industry for materials processing.[1,2] Many of the steps in integrated circuits (ICs) manufacturing, like etching and deposition of thin films are based on plasma processing.[1–3] When plasma is ignited, different reactions in gas phase and/or on surface may occur and new species like neutrals, radicals, excited species, ions, and stable etching products are created. The control of plasma chemistry, surface chemistry, and physical properties of ions reaching the surface is very critical. By adjustment and controlling of these properties, the desired functionality of the plasma processes, and an accurate and stable control of plasma reactor can be achieved. To improve the efficiency and performance of a plasma source, the main physics/chemistry of the discharge should be understood by using experiments and/or modeling and simulation.[4–6] To complement experiments, different numerical techniques, such as global model, fluid models, particle-in- cell, and hybrid models, are often used to estimate plasma optimum parameters.

In the semiconductor industry, different plasma reactors like capacitive couple plasma (CCP), inductive coupled plasma (ICP), and transformer coupled plasma (TCP) reactors have been designed, modeled, and understood to achieve the desired properties like etching and deposition, etc. Different gas mixtures and gas chemistries can be used for thin films deposition and etching. Various gas chemistries have been proposed to optimize the anisotropic dry etch process for different materials like ZnO thin films, Si- (Si_3N_4),Ga- (GaAs and GaN), and/or In-based (InP) materials.[7,8] The chemistry of chlorine (Cl_2, BCl_3) and hydrogen (CH_4, C_2H_6) containing plasmas has been adopted and investigated by researchers intensively.[9–13] The chlorine containing plasmas have the limitation due to low volatility of etching products. In these plasmas, the etching process mostly occurs in the ion-flux-limited etching regime.[11–13] In chlorine containing plasmas, high etch rate can be obtained by performing the etching process with wafers at high temperature (100 °C or above) along with stoichiometric composition of the etch surface. However, the high temperature of the wafer surface creates problems for the photoresist (PR) masks which results in high surface roughness. The surface roughness problem can be solved using hydrogen containing plasmas. These plasmas provide higher etch rates due to the formation of highly volatile metal-organic compounds. However, it has other problems like polymer deposition and hydrogen passivation of the etch surface, influencing the device performance.[9,10]

Recently, bromine-based (hydrogen bromide (HBr), Br_2) plasmas are being used and investigated to obtain stoichiometric composition of etch surface for the dry etching and the dry patterning of III–V In-based semiconductors (like InP and InGaAs).[14,15] Br-based plasmas provide much lower (compared with the Cl-containing plasmas) etch rates

a)E-mail: banatgul@gmail.com
b)E-mail: amansadiq@gmail.com

of organic PR. Halide (F, Cl, Br, I) selection for various material/thin films etching is the trade-off among multiple key players like etch rate, anisotropy, etch profile, etching selectivity, etc. For instance, HBr has attracted considerable attention in semiconductor industry recently[16–18] and has been widely employed in the plasma processing of integrated circuits for various applications like poly silicon etching, group III-V semiconductors, high k (dielectric constant) gate dielectrics, and low k oxides etching for interconnects. Higher etching anisotropy of single- and poly-crystalline silicon is clearly significant distinction of HBr containing plasmas due to negligible spontaneous reaction between Si surface and Br. It also provides higher etching selectivity in case of SiO_2, Si_3N_4, and organic photoresists. Furthermore, HBr plasma can be generated in combination of various buffer gases like Ar, Br_2, F_2, Cl_2, He, and H_2.[19–27] The chemistry of these discharges is therefore of great interest and understanding the main reactions involved in the generation of dominant species for etching is a first step in order to optimize the plasmas. By analyzing the published data, it can be concluded that most of the previous studies (especially for HBr/Ar discharge) were focused on the zero-dimensional global model[20–22,24,25] which provide no spatial information of species densities, fluxes, potential, and fields. In this work, we have developed a fluid model for HBr/He and HBr/Ar discharges. This model is able to capture spatial variations observed in an actual discharge, and is a powerful tool for identifying main species and reactions from a large set of chemical processes. In our work, we apply a self-consistent fluid model to conduct a comparative study of HBr/Ar and HBr/He plasmas in order to find the dominant species in the discharge for etching. The outline of this paper is as follows: Section II describes the fluid model along with reactions considered in the calculation. The simulation results along with discussion are presented in Section III. The conclusion of the paper is presented in Section IV.

II. MODEL AND REACTIONS

For the simulation, we developed a two-dimensional fluid code written in C language that runs in the LINUX system. It can calculate different plasma characteristics, including density, potential, electric field, power consumption, reaction rates, and the electron temperature. The simulation proceeds in real time and the CPU run time strongly depends on the number of species considered and gas pressure. For the considered plasma discharge, a CPU time of about 5–6 days is needed to get steady state solution. In this work, 15 different species have been considered for a gas mixture of HBr/He plasma discharge. The species considered in this model are electrons e, excited helium atoms He*, excited bromine atoms Br*, HBr*, HBr, He, hydrogen atom H, hydrogen molecule H_2, bromine atom Br, negative bromine ions Br^-, hydrogen atom ions H^+, hydrogen molecules ion H_2^+, bromine ions Br^+, hydrogen-bromide ions HBr^+, and helium ions He^+. Table I shows the reactions considered for HBr/He gas mixture.[22,25,28–33] The threshold energy for He* is19.8 eV. For HBr, three vibrational states and one electronic state are included, with energy thresholds of 0.3 eV, 0.6 eV, 0.9 eV, and 9.3 eV. The HBr/Ar gas mixture model also consists of 15 species in total; three species (argon ions Ar^+, excited argon atoms Ar*, electrons) belong to argon, while 12 species are related to HBr (these are the same as in case of HBr/He gas mixture). The reactions considered for HBr/Ar gas mixture are shown in Table II. It may be noted that the common reactions for HBr/Ar and HBr/He gas mixtures (given in Table I) are excluded from this list.

The rate of electron impact reactions, electron mobility, and diffusion coefficients is calculated by solving Boltzmann equation solver BOLSIG$^+$. The input data required for BOLSIG$^+$ were collected from literature. Specifically, the collision cross sections are taken from the references mentioned in Table I. It is noteworthy that HBr and its related reaction cross sections are not pre-registered in BOLSIG$^+$. We therefore edited the BOLSIG$^+$ input text file to include this desired cross section data (available in Ref. 34). With this modification, BOLSIG$^+$ was used to generate transport data (in the form of lookup tables) for different gas mixture ratios of HBr and buffer gas (He and Ar). The output data of BOLSIG$^+$ were saved in a text file and were afterwards provided to fluid code for computing the electron transport coefficients and

TABLE I. A list of reactions for HBr/He mixture.

No.	Reactions	Threshold (eV)/rate coefficients (cm^3s^{-1})	References
R1	$e + He \rightarrow He^* + e$	19.80	32
R2	$e + He \rightarrow He^+ + 2e$	24.54	32
R3	$e + He^* \rightarrow He^+ + 2e$	4.73	32
R4	$e + He^* \rightarrow He + e$	0.0	32
R5	$e + H_2 \rightarrow H + H + e$	8.8	30
R6	$e + H_2 \rightarrow H_2^+ + 2e$	15.43	36
R7	$e + H \rightarrow H^+ + 2e$	13.56	28
R8	$e + HBr \rightarrow HBr^* + e$	See text	34
R9	$e + HBr \rightarrow Br + H + e$	6.6	34
R10	$e + HBr \rightarrow Br^- + H$	0.08	34
R11	$e + HBr \rightarrow HBr^+ + 2e$	11.68	34
R12	$e + HBr^* \rightarrow HBr^+ + 2e$	11.68	34
R13	$e + HBr^* \rightarrow Br^- + H$	0.08	34
R14	$e + HBr^+ \rightarrow Br + H$	0.0	34
R15	$e + Br \rightarrow Br^* + e$	See text	31
R16	$e + Br \rightarrow Br^+ + 2e$	11.81	31
R17	$e + Br^- \rightarrow Br + 2e$	3.61	31
R18	$H + HBr \rightarrow H_2 + Br$	6.50×10^{-12}	22
R19	$Br^+ + HBr \rightarrow Br + HBr^+$	1.00×10^{-11}	c
R20	$H_2^+ + H \rightarrow H_2 + H^+$	6.40×10^{-10}	33
R21	$H_2^+ + N \rightarrow H_2 + N^+$	1.00×10^{-11}	c
R22	$H^+ + N \rightarrow H + N^+$	1.00×10^{-11}	c
R23	$Br^- + M^+ \rightarrow Br + M$[a]	1.00×10^{-7}	25
R24	$He^* + HBr \rightarrow H + Br + He$	5.00×10^{-12}	25
R25	$He^* + H_2 \rightarrow H + H + He$	5.00×10^{-12}	25
R26	$He^+ + N \rightarrow He + N^+$[b]	1.00×10^{-11}	c
R27	$He^+ + H \rightarrow He + H^+$	6.40×10^{-10}	37
R28	$He^+ + H_2 \rightarrow He + H_2^+$	1.00×10^{-11}	c
R29	$He^* + HBr \rightarrow He + HBr^+ + e$	8.00×10^{-10}	38
R30	$He^* + H_2 \rightarrow He + H_2^+ + e$	4.00×10^{-11}	38
R31	$He^* + He^* \rightarrow He^+ + He + e$	1.59×10^{-9}	32

[a]M = HBr, Br, H, H_2, He.
[b]N = HBr, Br.
[c]The rate coefficient is considered.

TABLE II. A list of reactions for HBr/Ar mixture.

No.	Reactions	Threshold (eV)/rate coefficients (cm^3s^{-1})	References
R1	$e + Ar \rightarrow Ar^* + e$	11.55	39
R2	$e + Ar \rightarrow Ar^+ + 2e$	15.76	36
R3	$e + Ar^* \rightarrow Ar^+ + 2e$	4.43	40
R4	$Ar^+ + X \rightarrow Ar + X^+$	1.00×10^{-11}	[b]
R5	$Br^- + X^+ \rightarrow Br + X$[a]	1.00×10^{-7}	25

[a]X = H, H_2, Br, HBr.
[b]The rate coefficient is considered.

source functions using standard relations.[35] The rates of the ion–ion, ion–neutral, and neutral–neutral reactions are determined by reaction rate coefficients taken from references mentioned in Tables I and II.

Note that in Tables I and II, several "general" reactions are indicated, which stand for several individual reactions occurring with different species (denoted by *M, N, and X*).

The plasma behaviour is described by the continuity equation, the momentum balance equation in the drift diffusion approximation for all the species, and the energy balance equation for electrons. The corresponding governing equations can be written as follows.

The particle balance for different species (electrons, ions and neutrals) is described by the continuity equation, i.e.,

$$\frac{\partial n_j}{\partial t} + \nabla \cdot \Gamma_j = S. \tag{1}$$

Here, n_j, Γ_j are the density and flux of particle j, while S is the source term. The momentum balance equation for all the species in the drift diffusion approximation is written as

$$\Gamma_j = -D_j \nabla n_j + \mu_j n_j \nabla V. \tag{2}$$

In above equation, μ_j, D_j are the mobility and diffusion coefficients of the jth species, respectively, while V is the electrostatic potential. The energy balance equation is solved for electrons only and is given by

$$\frac{\partial n_\varepsilon}{\partial t} + \nabla \cdot \ \Gamma_\varepsilon = S_\varepsilon, \tag{3}$$

where $n_\varepsilon = n_e \varepsilon$ is the electron energy density. The electron energy flux Γ_ε is given by

$$\Gamma_\varepsilon = -\frac{5}{3}\mu_e E n_\varepsilon - \frac{5}{3} D_e \frac{dn_\varepsilon}{dx}. \tag{4}$$

The electron energy source term is given by

$$S_\varepsilon = -e\Gamma_e \cdot \mathrm{E} - \mathrm{n}_e \sum_r \varepsilon_r k_r n_r. \tag{5}$$

In Eq. (5), the first term represents the electron heating by electric field, while the second term represents the energy lost in collision, n_r is the density of the target particle, and ε_r is the threshold energy for a collision of type r. For self-consistent calculation of the electric fields, above equations are coupled with Poisson's equations

$$\nabla \cdot (\epsilon \nabla V) = -\sum q_p n_p. \tag{6}$$

Poisson equation is solved with a successive over relation (SOR) method. The electric field is taken at time t when the continuity equations are integrated between t and $t + \Delta t$. Alternating Direction Implicit (ADI) method is used to integrate the continuity equation. ADI method uses two time steps in two dimensions to update the quantities between t and $t + \Delta t$. The equation of continuity is solved numerically with the semi-implicit Scharfetter-Gummel exponential scheme. In this numerical scheme, it is assumed that the particle flux is calculated at the grid points by taking it constant between half grid points. The electron density is calculated at the centre of the cell and the potential is calculated at the grid points. The system of equations described above is complemented by a set of boundary conditions on the densities and fluxes of the species involved and the electric potential. The electric potential at the high frequency (HF) driven electrode and grounded electrode is defined, respectively, as

$$V_{rf} = V_0 \sin(2\pi f t) \text{ and } V_{ground} = 0. \tag{7}$$

Here, V_0 and f are the amplitudes and frequencies of the driving power sources, respectively. The boundary conditions for the particle fluxes at the boundary of the plasma are

$$\begin{aligned} \Gamma_j \cdot n &= \mu_j n_j E \cdot n + n_j \frac{v_{th,j}}{4} \\ \Gamma_e \cdot n &= -\mu_j n_j E \cdot n + n_e \frac{v_{th,e}}{4} - \sum_{i,ex} \gamma_{i,ex} \Gamma_{i,ex} . n \\ \Gamma_{ex} \cdot n &= n_{ex} \frac{v_{th,ex}}{4}, \end{aligned} \tag{8}$$

$\gamma_{i,ex}$ is the secondary electron emission coefficient for the particle of type i, ex, and υ_{th} is the thermal velocity. In the case of the density of electrons, a flux due to secondary emission by ion or metastable impact is added to the flux defined by Eq. (8).

The diffusion and mobility coefficients for electrons are calculated by using Boltzmann solver BOLSIG$^+$. The mobility $\mu_{i,j}$ (in units of $m^2s^{-1}V^{-1}$) of the jth ion in the ith background neutral gas is calculated using low field Langeving mobility expression given by[41,42]

$$\mu_{i,j} = 0.514 \frac{T_g}{(m_{i,j}\alpha_i)^{0.5} P_{tot}}. \tag{9}$$

The ion mobility in the background gas mixture is obtained by using the Blanc's law

$$\frac{P_{tot}}{\mu_i} = \sum_i \frac{P_i}{\mu_{i,j}}. \tag{10}$$

The diffusion coefficients for ions are calculated by using the Einstein relation

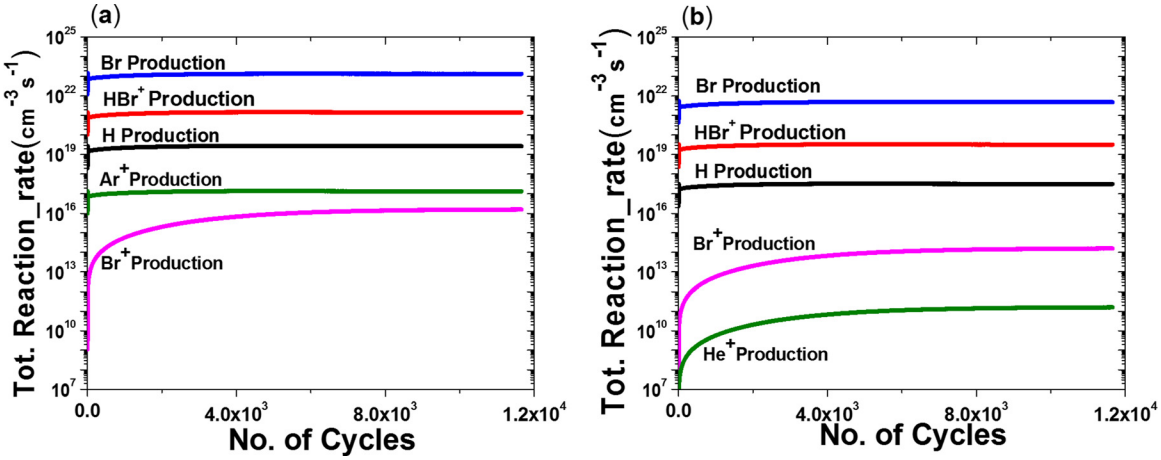

FIG. 1. Time average total reaction rates of the reactions involved in the production of H, Br, Br^+, HBr^+ Ar^+, and/or He^+ in HBr/Ar plasma(0.8/0.2) (a) and HBr/He plasma(0.8/0.2) (b). The operating conditions are total gas pressure 50 mTorr, electrode gap 3 cm, and operating frequency13.56 MHz.

$$D_j = \frac{k_B T_{gas}}{e}\mu_j. \tag{11}$$

The diffusion coefficient $D_{i,j}$ (in units of $m^2s^{-}1$) for the jth neutral species in the ith background gas component is obtained by using the binary relation[41]

$$D_{i,j} = \frac{3k_B T_{gas}}{16P_{tot}} \frac{\sqrt{\frac{2\pi k_B T_{gas}}{m_{i,j}}}}{\pi\sigma_{i,j}^2 \Omega_D(\Psi)}. \tag{12}$$

In Eqs. (9) and (10), P_{tot} is the total gas pressure, α_i is the polarizability of ith gas molecules, T_g is the gas temperature, $m_{i,j}$ is the reduced mass, and P_i is the partial gas pressure of the ith background gas component. In Eqs. (11) and (12), k_B is the Boltzmann constant, $\Omega_D(\Psi)$ is the diffusion collision integral with $\Psi = T_{gas}/\varepsilon_{i,j}$ and $\varepsilon_{i,j} = \sqrt{\varepsilon_i \times \varepsilon_j}$ and $\sigma_{i,j} = (\sigma_i + \sigma_j)/2$ is the binary collision diameter, where ε_j and σ_j are the Lenard-Jones parameters. The diffusion coefficient D_i in the background gas mixture is obtained by using the Blanc's law similar to Eq. (11).

III. RESULTS AND DISCUSSION

As mentioned above, the main focus of this study is to identify the dominant species in HBr plasmas using time average reaction rates calculations by fluid model and to investigate the effect of buffer gases (He and Ar) on the flux and density distribution of these active species. The simulation of CCP reactor is performed with discharge gap of Z = L = 3 cm and electrode radius of R = 15 cm. The driving frequency is taken to be 13.56 MHz, operating voltage is 300 V, and total pressure of background gasses is 50 mTorr. The working gas for initial simulation is 20% He or Ar, and 80% HBr mixture.

The simulation results showed that the dominant species in both HBr/He and HBr/Ar plasmas are Br, H, Br^+, and HBr^+. In both HBr/Ar and HBr/He plasmas, the neutral species H and Br are mainly produced from the dissociation of HBr through reactions R9–R10 and R13–R14. In addition, these species can also be produced via step dissociation of He* through reactions R24 and R25 in HBr/He plasma. The rates of these reactions are very high which results in high densities of H and Br in the discharge. Similarly, Ar^+/He^+, HBr^+, and Br^+ are generated in the discharge through the direct ionization of Ar and/or He, HBr, and Br through reactions R2–R3, R11–R12, R16. These ions are also produced in the discharge through other reactions/processes like R21–R22, R26, and R29. The total reaction rate for the production of all the dominant and active species is shown in Figure 1.

The most dominant and active species that play a vital role in the etching process in the HBr plasmas are reactive neutrals H and Br atoms which are the main precursors for chemical etching as well as the ions like HBr^+ and Br^+ which are responsible for sputtering of the substrate. Figure 2 shows a comparison of the density distributions of the active neutral species (H and Br) in both the plasmas. The high densities of H and Br in the discharge clearly indicate that HBr is highly dissociative. The active neutral species (H and Br) shown in this figure have bell shaped distribution which indicates that these species have higher generation rate than consumption rate at the center of discharge. This figure also shows that the densities of H and Br in HBr/Ar plasmas are an order of magnitude higher than the densities of these species in HBr/He plasmas. This is due to low excitation and ionization energy of Ar as compared to He. The low excitation and ionization energy of Ar result in production of more electrons in HBr/Ar as compared to HBr/He plasma and hence higher production rates of these active species through dissociation and ionization phenomena.

Figure 3 shows a comparison of the active ionic species produced in the HBr/Ar and HBr/He plasmas. The most prominent ions in both the discharges are HBr^+, Br^+, Br^-, He^+, and/or Ar^+. The densities of other ions like H^+, H_2^+ are comparatively small and are not shown. The ions HBr^+ and Br^+ have double humped density distribution in the discharge which shows that these ions are mostly produced near the electrodes. The HBr^+ density is higher than all other positive ions in both the discharges. However, the densities of

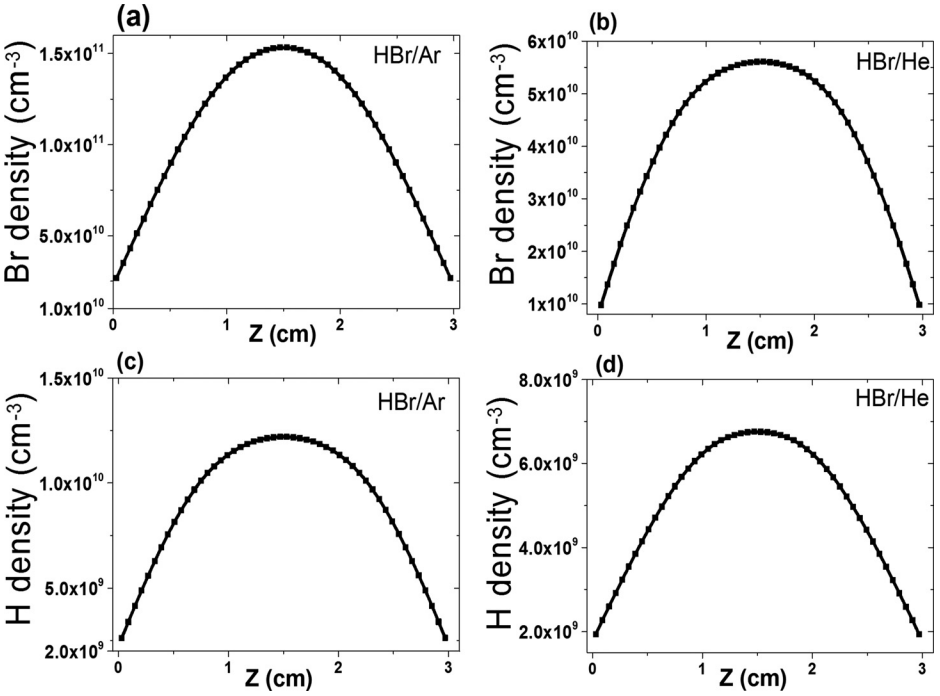

FIG. 2. Distributions of the active neutral species densities in HBr/Ar and HBr/He (0.8/20) discharge for the same operating conditions as in Figure 1.

all the ions in HBr/Ar plasma are higher an order of magnitude than the densities of ions in HBr/He plasma for the same reason as discussed above and are shown in Figure 3. Moreover, it may be noted that in HBr plasmas, Br^- is formed by electron impact dissociative attachment of HBr (R10 and R13 in Table I), which has a very low threshold energy of about 0.08 eV, therefore Br^- has high density (about 10^{11} cm^{-3}) in both the discharges as shown in Figure 4 for HBr/Ar discharge. HBr^+ and Br^+ density distribution are more uniform in the center of the discharge in HBr/Ar plasmas which shows these ions are consumed at relatively low rate and therefore have relative high densities compare to HBr/He plasmas.

Figure 5 shows the pattern of electric field and power density distribution for HBr/Ar (0.8/0.2) plasma. The electric field is relatively weak in the bulk plasma region while rapidly increases towards the electrodes and radial edge, suggesting the predominant ionization in these regions. Consequently, the delivered power would primarily dissipate in the aforementioned regions, as shown by Figs. 5(c) and 5(d).

Figures 6(a) and 6(b) show the space averaged densities of the active etchant species, i.e., Br, HBr^+, H, and Br^+ in HBr/Ar and HBr/He plasma as a function of additive gas (Ar or He) fraction. These species are considered to be important for etching in HBr-based discharges.[43] The densities of Br, HBr^+, and H decrease slightly by increasing concentration of the buffer gas (i.e., He or Ar) in the discharge. In both the plasmas, Br^+, He^+, and/or Ar^+ densities increase with increase in concentration of the additive gas. Furthermore, it can be seen from Figure 6 that the densities of all dominant species, i.e., Br, H, Br^+, HBr^+ in HBr/Ar discharge are slightly higher an order of magnitude than those in HBr/He discharges for the same input parameters and same reason as explained earlier.

Figure 7 shows the electron density and electron temperature as a function of additive gas percentage for HBr/Ar and HBr/He plasma discharges. As the additive gas He or Ar fraction increases, the density and temperature of electrons increased in both HBr/Ar and HBr/He plasmas. Compare to HBr and Br, the electron impact reactions for Ar and/or He have higher threshold energies (See Tables I and II) or lower cross-section and therefore will not occur so often. This results in an increase in the electron temperature with addition of He or Ar to HBr as shown in Figure 7(b). The increase in temperature of electrons allows more ionization and excitation. The electron impact ionization is the main production process for the electrons which results in an increase in the density of electrons. However, the density of electrons in HBr/Ar is higher than that in HBr/He for same input parameters, as shown in Figure 7(a). This may be due to the lower excitation and ionization threshold energies of Ar (11.6 and 15.8 eV, respectively) than that of He (19.8 and 24.6 eV, respectively). Furthermore, the electron temperature in HBr/He plasma is relatively high than HBr/Ar plasma. This is due to the higher threshold energies for the electron impact reactions of He (24.54 eV). This results in less energy transfer from electrons to He gas atoms in case of HBr/He plasma. Similar trends have also been observed with the Langmuir probe diagnostics reported by Ham *et al.*[21] and by others.[43,44]

Figure 8 shows the radial distribution of the species densities and fluxes in HBr/Ar plasma. It can be seen that all the species are uniformly distributed along the wafer surface (on electrode). The maximum density of HBr^+, Ar^+, H, and Br species appears near the ground side wall of the reactor, where more electron impact ionization (of Ar and HBr) and dissociation (of HBr) occur due to the strong electric filed near the reactor edge (see Figure 5). The stronger electric field gives high electron density near the reactor edge. The

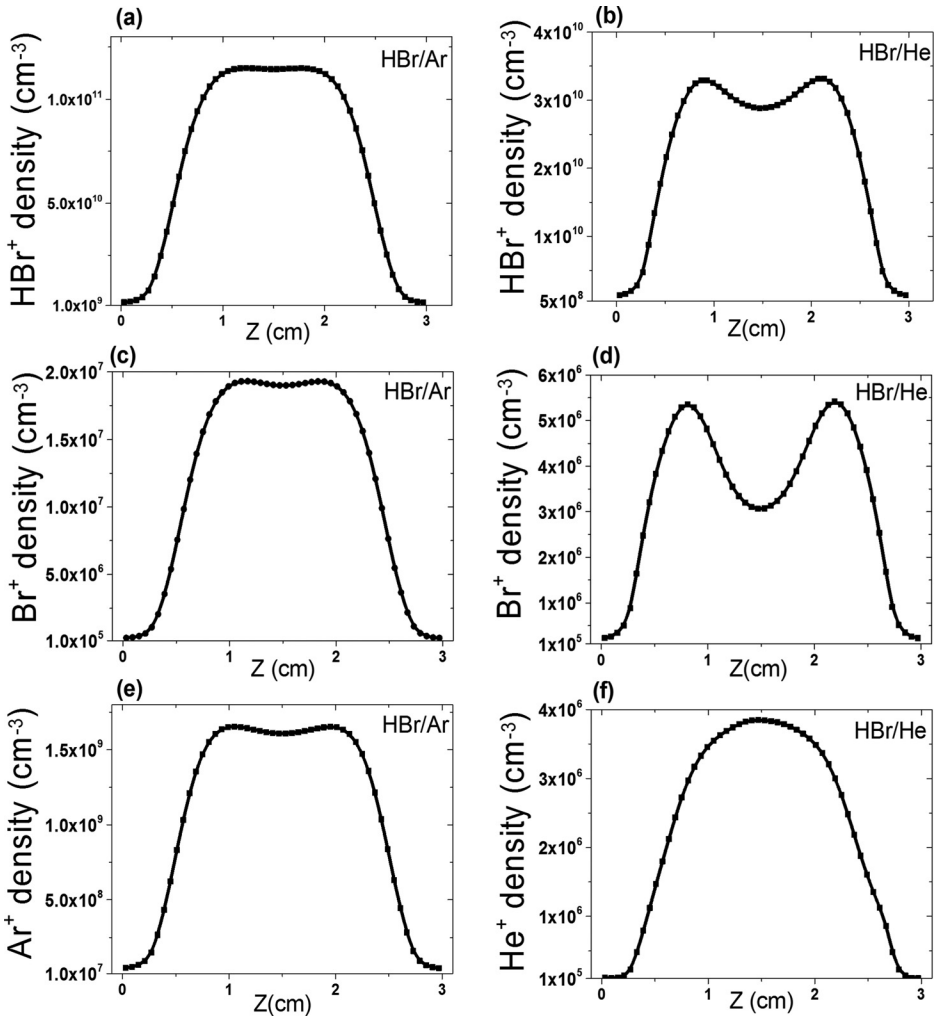

FIG. 3. Distributions of the active ion species densities in HBr/Ar and HBr/He (0.8/20) discharge for the same operating conditions as in Figure 1.

electron density distribution clearly affects the radial distribution in densities of HBr^+, Ar^+, H, and Br. In fact, all these species are produced mainly by electron impact ionization and dissociation, as stated above. The uniform density distribution of dominant/active species along radius/wafer can lead to uniform and controlled etching pattern of the wafer, therefore by suitable gas ratio of HBr plasmas, the uniform and controlled etching can be achieved.

As in HBr plasmas, H, Br, Br^+, HBr^+, and Ar^+/He^+ species have an important influence on the etch process, the radial distribution of the axial flux of these species along with fluxes of background gas species (HBr and Ar for HBr/Ar plasma) at the wafer surface (electrode) is presented in Figure 8(b). It can be observed that the flux of Br^+ is few order lower than the flux of Ar^+ and HBr^+ for the same operating condition. The maximum flux of HBr^+, Ar^+, H, and Br species appears near the ground side wall. The radial flux of Br^- is around $10^{15}\,cm^{-2}s^{-1}$ and is not shown in the figure. From Figure 8(b), it is clear that the flux of neutrals is around $10^{18}\,cm^{-2}s^{-1}$, while the flux of the ions in the plasma is about $10^{15}\,cm^{-2}s^{-1}$. This means that more neutrals are arriving at the electrode (wafer surface) than the ions which are logical for the considered operating conditions of CCP plasma.

The densities of active species in HBr/He plasma are lowered by an order of magnitude or more from HBr/Ar plasma (Figure 6), so the same trend of radial distribution of active species densities and/or fluxes is obtained for HBr/He

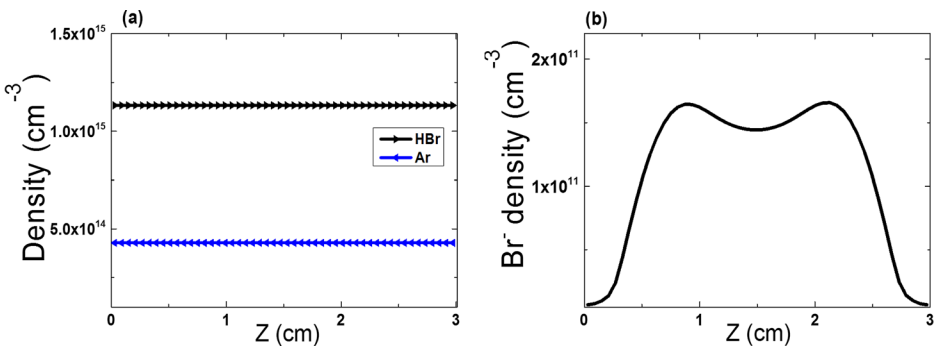

FIG. 4. Density distributions of other relevant species in HBr/Ar (0.8/20) discharge for the same operating conditions as in Figure 1.

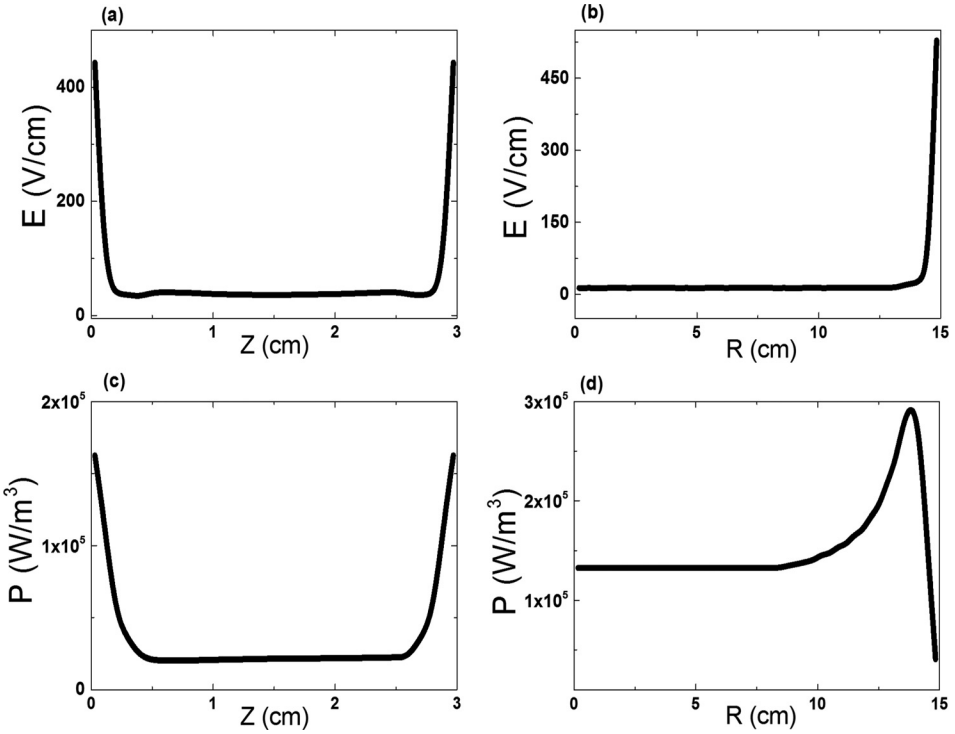

FIG. 5. The distribution of average electric field and average power density for HBr/Ar (0.8/0.2) plasma. Axial filed distribution at the center of the discharge (a), radial field distribution near the electrode surface (b), axial power density distribution at the center (c), radial power density distribution near the electrode surface (d). The other operating conditions are the same as in Figure 1.

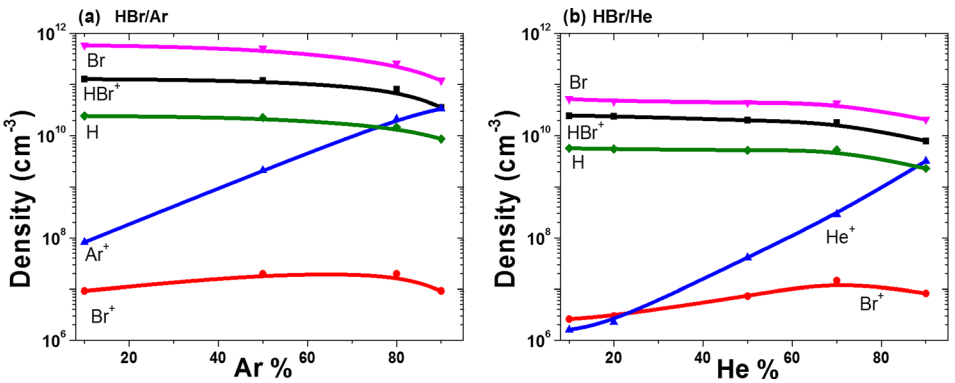

FIG. 6. Densities of the active etchant neutrals and positive ions species as a function of additive gas fraction in the HBr/Ar plasma (a) and HBr/He plasma (b). The other operating conditions are the same as in Figure 1.

plasma (not shown) but with 1–3 orders of magnitude small. Furthermore, as with the increase in the additive gas fraction in HBr, the densities of ions like Ar^+/He^+ and Br^+ increase, therefore it is logical that the ratio of active ions density(or flux) vs. active neutrals density(or flux) will increase. The density and flux of Ar^+ in HBr/Ar plasma is a few order of magnitude greater than the density and flux of He^+ in HBr/He plasma, therefore compared to HBr/He plasma, a maximum change (increase) in ions vs. neutrals density (or flux) occurs for HBr/Ar plasma.

In order to improve and control the etching uniformity and etch rate, it is important to control the densities and fluxes of the active etchant species in the discharge and on the electrode surfaces (wafer). To do so, different input parameters like gas pressure, excitation frequency, applied voltage, discharge gap, gas mixture ratio, etc., can be used to

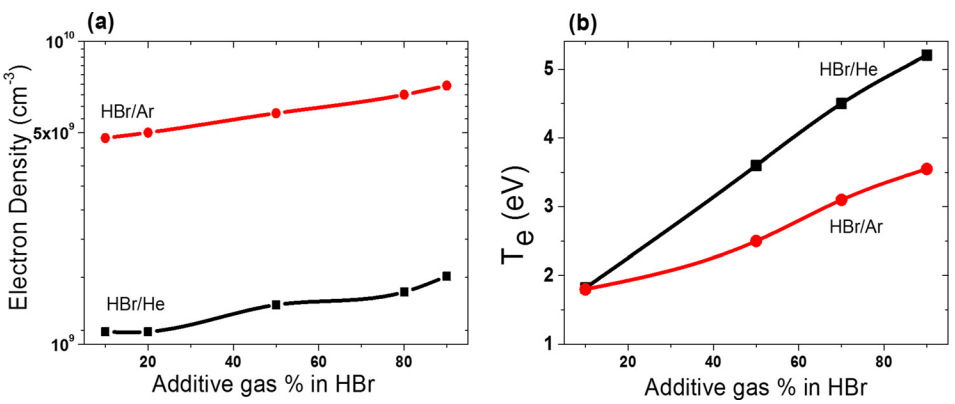

FIG. 7. The electron density (a) and electron temperature (b) of HBr/Ar and HBr/He as a function of additive gas fraction. The other operating conditions are the same as in Figure 1.

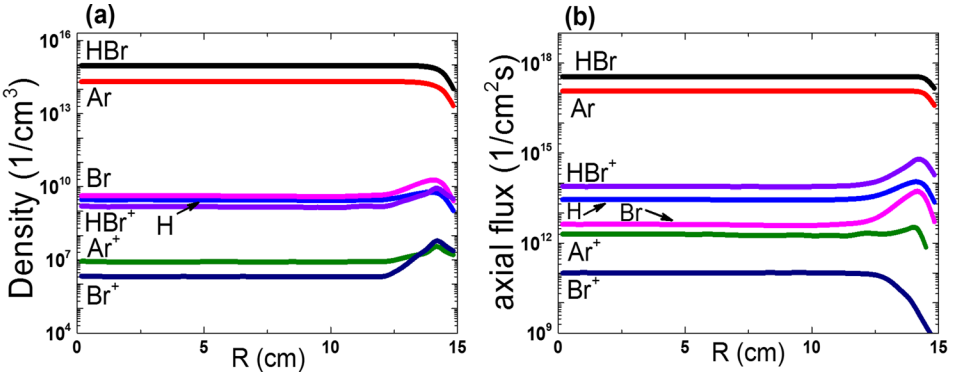

FIG. 8. Radial distribution of species densities (a) and species fluxes (b) near the powered electrode (wafer) in HBr/Ar (0.8/0.2) plasma. The other operating conditions are the same as in Figure 1.

control the densities and fluxes of these dominant species. Out of all these input parameters, the main variable which controls the densities and fluxes of various species is the gas mixture ratio (HBr/X, X = Ar or He) to control the etchant species densities and hence their fluxes in the discharge. Both the amounts of precursors gas HBr and ionizing agent X change as a function of additive gas fraction, so we can expect a variation in the chemical composition and other reactive species in the discharge. With the increase in the additive gas percentage in HBr, the H and Br density decreases (Fig. 6). These etchant atoms delivered from the discharge react with the electrode surface (wafer) to form volatile etch products. The higher the densities and fluxes of these etchant atoms, the more volatile etch products are formed and the higher etch rate is achieved. The decrease in densities and fluxes of these species indicates that chemical etch rate decreases upon increasing additive gas fraction. On the other hand, the ions like X^+ and Br^+ densities (and hence their fluxes) increase with the increase in additive gas fraction in the plasma. The higher densities (and fluxes) of ions in the plasma are needed for anisotropic etching. As the additive gas fraction increases, the ions to neutral flux (or density) ratio increases. However, the density of Ar^+ in HBr/Ar is 3–4 orders higher than He^+ in HBr/He plasma (Figure 6), therefore HBr/Ar plasma shows more change in the ion density and flux as compared to HBr/He plasma and hence the etching rate in HBr/Ar plasma discharge can be considered to be in the ion-assisted regime. The overall density of H and Br in HBr/X plasma is higher than Br^+ and HBr^+ densities. This suggest that the chemical etching is prominent than physical etching and hence the overall etch rate decreases upon increasing additive gas fraction in HBr plasma. The decrease in etch rate in HBr plasmas upon increase in the additive gases fraction (He, Ar, Cl_2, N_2, O_2, etc.) has been reported in the literature.

IV. CONCLUSIONS

HBr has been widely used in the semiconductor industry for various applications like poly silicon etching, group III-V semiconductors, high k (dielectric constant) gate dielectrics, and low k oxides etching for interconnects. HBr plasma also provides higher etching selectivity in case of SiO_2, Si_3N_4, and organic photoresists. It is therefore important to identify the active species in the HBr plasma discharge and to estimate the densities of neutral species and ions that play a crucial role in the etching process under various operating conditions.

In this paper, extensive sets of gas-phase reactions for modeling of HBr/He and HBr/Ar plasma discharges are constructed. These sets include various processes like ionization, excitation, and dissociation and also the reactions of neutrals, radicals, and ions. The model calculations shows that the most dominant species for etching in HBr/Ar and HBr/He discharge are HBr^+, Br^+, Br, and H. In the HBr plasma, neutral species like H and Br are the key players for chemical etching, while positive ions like Br^+ and HBr^+, He^+, and/or Ar^+ are responsible for physical and ion-assisted etching.

As the fraction of additive gas mixture is increased in HBr, the electron density and the electron temperature are increased. The densities of all species in HBr/Ar plasma are higher than those of HBr/He plasma, however, the electron temperature of HBr/He is higher than that of HBr/Ar. It was found that with increase in additive gas fraction, the densities of neutral species H and Br decrease slightly, while the densities of ions Br^+ and He^+/Ar^+ increases more quickly. Therefore, the ions to neutral density ratios change which is a key for the selective and anisotropic etching in HBr plasma. Since the Ar^+ density in HBr/Ar plasma is 3–4 times higher than He^+ density in HBr/He discharge, the ratio of active ions to neutral species densities is very high in HBr/Ar discharge and hence enhanced anisotropic etching can be obtained with HBr/Ar plasma discharge. Moreover, higher fraction of the additive gas results in higher positive ion densities and fluxes towards the substrate, and hence a uniform and anisotropic etching profile can be obtained.

ACKNOWLEDGMENTS

The author would like to thank the Higher Education Commission of Pakistan (HEC) for financial support under the Indigenous PhD Programme. Authors are grateful to O. Šašić (Institute of physics, Belgrade, Serbia) for provision of electrons cross section and transport coefficient data of HBr for this study.

[1]R. D'Agostino, P. Favia, C. Oehr, and M. R. Wertheimer, Plasma Process. Polym. **2**, 7 (2005).
[2]H. M. Anderson, NATO ASI Ser. **290**, 1 (1995).
[3]B. Radjenović and M. Radmilović-Radjenović, Cent. Eur. J. Phys. **9**, 265 (2011).
[4]H. C. Kim, F. Iza, S. S. Yang, M. Radmilović-Radjenović, and J. K. Lee, J. Phys. D. Appl. Phys. **38**, R283 (2005).
[5]D. B. Graves and P. Brault, J. Phys. D: Appl. Phys. **42**, 194011 (2009).

[6]J. van Dijk, G. M. W. Kroesen, and A. Bogaerts, J. Phys. D: Appl. Phys. **42**, 190301 (2009).
[7]H. Kupfer, R. Kleinhempel, B. Graffel, T. Welzel, T. Dunger, F. Richter, W. M. Gnehr, and T. Kopte, Surf. Coat. Technol. **201**, 3964 (2006).
[8]A. B. Djurišić, C. Y. Kwong, P. C. Chui, and W. K. Chan, J. Appl. Phys. **93**, 5472 (2003).
[9]L. Ji-Myon, C. Ki-Myung, K. Kyoung-Kook, C. Won-Kook, and P. Seong-Ju, J. Electrochem. Soc. **148**, G1 (2001).
[10]M. H. Shin, M. S. Park, S. H. Jung, J. H. Boo, and N. E. Lee, Thin Solid Films **515**, 4950 (2007).
[11]S. W. Na, M. H. Shin, Y. M. Chung, J. G. Han, S. H. Jeung, J. H. Boo, and N.-E. Lee, Microelectron. Eng. **83**, 328 (2006).
[12]H.-K. Kim, J. W. Bae, T.-K. Kim, K.-K. Kim, T.-Y. Seong, and I. Adesida, J. Vac. Sci. Technol., B: Microelectron. Nanometer Struct.–Process., Meas., Phenom. **21**, 1273 (2003).
[13]J.-W. Bae, C.-H. Jeong, H.-K. Kim, K.-K. Kim, N.-G. Cho, T.-Y. Seong, S.-J. Park, I. Adesida, and G.-Y. Yeom, Jpn. J. Appl. Phys. Part 2 **42**, L535 (2003).
[14]S. J. Pearton, U. K. Chakrabarti, E. Lane, A. P. Perley, C. R. Abernathy, W. S. Hobson, and K. S. Jones, J. Electrochem. Soc. **139**, 856 (1992).
[15]K. Yue and T. L. Tai, J. Electrochem. Soc. **145**, 4313 (1998).
[16]N. Layadi, J. I. Colonell, and J. T. Lee, Bell Labs Tech. J. **4**(3), 155 (1999).
[17]A. P. Mahorowala, H. H. Sawin, R. Jones, and A. H. Labun, J. Vac. Sci. Technol., B: Microelectron. Nanometer Struct.–Process., Meas., Phenom. **20**, 1055 (2002).
[18]L. Desvoivres, L. Vallier, and O. Joubert, J. Vac. Sci. Technol., B: Microelectron. Nanometer Struct.–Process., Meas., Phenom. **18**, 156 (2000).
[19]S. Bouchoule, L. Vallier, G. Patriarche, T. Chevolleau, and C. Cardinaud, J. Vac. Sci. Technol., A **30**, 031301 (2012).
[20]A. Efremov, Y. Kim, H. Lee, and K. Kwon, Plasma Chem. Plasma Process. **31**, 259 (2011).
[21]Y.-H. Ham, A. Efremov, H. W. Lee, S. J. Yun, N. K. Min, K.-H. Baek, L.-M. Do, and K.-H. Kwon, Vacuum **85**, 1021 (2011).
[22]Y. H. Ham, A. Efremov, S. J. Yun, J. K. Kim, N. K. Min, and K. H. Kwon, Thin Solid Films **517**, 4242 (2009).
[23]D. W. Kim, C. H. Jeong, K. N. Kim, H. Y. Lee, H. S. Kim, and G. Y. Yeom, J. Korean Phys. Soc. **42**, 795 (2003), www.corial.net/resources/pdf/sapphire_etching.pdf.
[24]H. W. Lee, M. Kim, N.-K. Min, A. Efremov, C.-W. Lee, and K.-H. Kwon, Jpn. J. Appl. Phys. Part 1 **47**, 6917 (2008).
[25]A. A. Smirnov, A. M. Efremov, and V. I. Svettsov, Russ. Microelectron. **39**, 418 (2010).
[26]I. W. Rangelow, J. Vac. Sci. Technol., B: Microelectron. Nanometer Struct.–Process., Meas., Phenom. **13**, 2394 (1995).
[27]V. Srivastav, R. Pal, and H. P. Vyas, Opto-Electron. Rev. **13**, 197 (2005), https://www.infona.pl/resource/bwmeta1.element.baztech-article-BWA0-0002-0054/tab/summary?locale=en.
[28]P. Banks, Planet. Space Sci. **14**, 1085 (1966).
[29]A. Bogaerts, E. Neyts, R. Gijbels, and J. van der Mullen, Spectrochim. Acta, Part B **57**, 609 (2002).
[30]S. J. B. Corrigan, J. Chem. Phys. **43**, 4381 (1965).
[31]M. J. Kushner, J. Phys. D: Appl. Phys. **42**, 194013 (2009).
[32]S. Rauf and M. Kushner, J. Appl. Phys. **85**, 3460 (1999).
[33]M. J. Kushner, J. Appl. Phys. **63**, 2532 (1988).
[34]O. Šašić, S. Dujko, T. Makabe, and Z. L. Petrović, Chem. Phys. **398**, 154 (2012).
[35]G. J. M. Hagelaar and L. C. Pitchford, Plasma Sources Sci. Technol. **14**, 722 (2005).
[36]D. Rapp and P. Englander-Golden, J. Chem. Phys. **43**, 1464 (1965).
[37]E. Carrasco, M. Jiménez-redondo, I. Tanarro, and V. J. Herrero, Phys. Chem. Chem. Phys. **13**, 19561 (2011).
[38]C. B. Collins and F. W. Lee, J. Chem. Phys. **70**, 1275 (1979).
[39]K. Tachibana, Phys. Rev. A **34**, 1007 (1986).
[40]S. Tinck, W. Boullart, and A. Bogaerts, J. Phys. D: Appl. Phys. **42**, 095204 (2009).
[41]J. Perrin, O. Leroy, and M. Bordage, Contrib. Plasma Phys. **36**, 3 (1996).
[42]Aman-Ur-Rehman, H. C. Kwon, W. T. Park, and J. K. Lee, Phys. Plasmas **18**, 093502 (2011).
[43]B. Gul, S. Tinck, P. De Schepper, A. Rehman, and A. Bogaerts, J. Phys. D: Appl. Phys. **48**, 025202 (2015).
[44]C. C. Cheng, J. Vac. Sci. Technol., B: Microelectron. Nanometer Struct.–Process., Meas., Phenom. **14**, 85 (1996).